1

Magnetic field generation by fluid dynamos

{ch:Dynamo}

The solar magnetic field is the engine and energy source powering all phenomena that collectively define what we call solar activity. The cyclic regeneration of this magnetic field is now generally understood to be driven by a hydromagnetic dynamo operating somewhere in the solar interior, through the inductive action of fluid flows. However, some important aspects of the physical processes involved remain elusive, notably the mechanism(s) regulating the primary cycle's amplitude and period, the physical origin of cycle-to-cycle fluctuations in overall activity levels, and the underlying causes of modulations on long timescales, including the extended periods of strongly reduced magnetic activity.

Astrophysical dynamo theory is an immense topic, which is the subject of numerous recent and not-so-recent monographs (e.g., Moffatt, 1978; Parker, 1979; Krause and Rädler, 1980; Rüdiger and Hollerbach, 2004; Charbonneau, 2013; Moffatt and Dormy, 2019), as well as a number of extensive review articles (e.g. Ossendrijver, 2003; Brandenburg and Subramanian, 2005; Charbonneau, 2014). This chapter aims at establishing the basic physical principles underlying magnetic field generation by astrophysical fluid dynamos. The design and behavior of specific solar cycle models will be discussed at length in chapters 2 and 3.

1.1 Magnetohydrodynamical dynamo action

At the microscopic level, solar plasma is made up of an electrically neutral mixture of electrically-charged constituents: electrons, Hydrogen and Helium nucleii, and small quantities of heavier ions. In the solar interior up to the photosphere, the number densities and thermal speeds are high enough for collision frequencies to largely exceeds any other relevant plasma frequencies. Under such physical conditions, at the macroscopic level the interaction

of fluid flow and magnetic field is well-described by the magnetohydrodynamical approximation (hereafter MHD; see, e.g., Davidson, 2001). It is this interaction that leads to the cyclic regeneration of the solar magnetic field by dynamo action.

{ssec:mhd}

1.1.1 The MHD induction equations

The starting point towards magnetohydrodynamical induction is Maxwell's equations, and more specifically Faraday's Law:

Faraday's Law

{eq:Faraday}

$$\frac{\partial \mathbf{B}}{\partial t} = -\nabla \times \mathbf{E} \ , \tag{1.1}$$

where $\mathbf{E}$ [V m^{-1}] and $\mathbf{B}$ [T] are the electric and magnetic fields, respectively (SI units are used throughout). In a collisionally-dominated plasma flowing at speed $\mathbf{u}$ at the macroscopic scale, Ohm's Law is expected holds in a reference frame co-moving with the flow:

{eq:Ohm}

$$\mathbf{J}' = \sigma \mathbf{E}' \ , \tag{1.2}$$

where $\mathbf{J}$ [A m^{-2}] is the electric current density, primed quantities denote measures made in the comoving frame, and σ [Ohm m^{-1}, $\equiv$ C^{2}s^{-1}m^{-3}kg^{-1}] is the electrical conductivity. For a non-relativistic fluid flow $\mathbf{u}$, Lorentz transformation to the rest frame reduces to $\mathbf{J}' = \mathbf{J}$ and $\mathbf{E}' = \mathbf{E} + \mathbf{u} \times \mathbf{B}$. Substituting in Ohm's Law then yields an expression for the rest frame electric field:

Generalized Ohm's Law

{eq:mhd1}

$$\mathbf{E} = \mathbf{J}/\sigma - \mathbf{u} \times \mathbf{B} \ . \tag{1.3}$$

Excluding externally imposed rapid variations of $\mathbf{E}$, Ampère's law holds in its pre-Maxwellian form:

Ampère's Law

{eq:mhd2}

$$\nabla \times \mathbf{B} = \mu_0 \mathbf{J} \ , \tag{1.4}$$

where $\mu_0 = 4\pi \times 10^{-7}$ N A^{-2} is the magnetic permeability. Using this expression to substitute for $\mathbf{J}$ in eq. (1.3), and inserting the resulting expression for $\mathbf{E}$ on the RHS of eq. (1.1) leads to the *MHD induction equation*:

{eq:mhd}

$$\frac{\partial \mathbf{B}}{\partial t} = \nabla \times (\mathbf{u} \times \mathbf{B} - \eta \nabla \times \mathbf{B}) \ , \tag{1.5}$$

where $\eta = (\mu_0 \sigma)^{-1}$ [m^2 s^{-1}] is the *magnetic diffusivity*. The first term on the RHS expresses induction by the flow of electrically charged constituents across the magnetic field, and the second Ohmic dissipation of the current systems supporting that same magnetic field, as per eq. (1.4). The MHD induction equation is the mathematical and physical cornerstone of magnetic field generation in electrically conducting fluids, i.e., *fluid dynamos*

Magnetic diffusivity

Fluid dynamo

{ssec:scaling}

1.1.2 Timescales and the magnetic Reynolds number

The relative importance of induction versus dissipation, and associated timescales, can be estimated by dimensional analysis of eq. (1.5). Assume that it is possible to identify *a priori* a characteristic values u_0 for the flow speed, and L for a length scale adequately characterizing the spatial variations of both the flow and magnetic field. Replacing spatial differential operators by $1/L$ and temporal derivatives by $1/\tau$ in eq. (1.5) leads to:

$$\frac{1}{\tau} \sim \frac{u_0}{L} - \frac{\eta}{L^2} \ . \tag{1.6}$$ {eq:mhddim}

The ratio of the first to second term on the RHS of eq. (1.6) yields a measure of the relative importance of induction versus dissipation. This dimensionless ratio is known as the *Magnetic Reynolds number*:

Magnetic Reynolds number

$$\mathrm{Rm} = \frac{u_0 L}{\eta} \ . \tag{1.7}$$ {eq:Rm}

With the magnetic diffusivity $\eta \sim 1\,\mathrm{m^2\,s^{-1}}$ for the bulk of the solar convection zone, $u_0 \sim 10\,\mathrm{m\,s^{-1}}$ for deep convection, and L set equal to the solar radius $R_\odot = 6.96 \times 10^8\,\mathrm{m}$, we get $\mathrm{Rm} \sim 10^{10}$, indicating that Ohmic dissipation is very inefficient on global solar scales. Note that this is not so much because u_0 is particularly large or η very small —copper is a much better electrical conductor than the plasma in the solar interior,— but is instead a consequence of the large spatial scale of the system. Equation (1.6) also yields two natural timescales for magnetic field evolution, namely the *advective timescale*:

Advection time

$$\tau_u = L/u_0 \ , \tag{1.8}$$ {eq:tadvec}

and the *diffusive timescale*:

Diffusion time

$$\tau_\eta = L^2/\eta \ . \tag{1.9}$$ {eq:tdiff}

Note that under these definitions $\mathrm{Rm} \equiv \tau_\eta/\tau_u$. Using the same numerical values as above, we get $\tau_u \simeq 1\,\mathrm{yr}$ and $\tau_\eta \simeq 10^{10}\,\mathrm{yr}$, the latter twice the age of the Sun. The very long diffusive timescale implies that we must look to the flow $\mathbf{u}$ to explain the much shorter evolutionary timescales observed, from the decadal cycle period, down to minutes for the evolution of small photospheric magnetic flux concentrations.

The electrical current density required to sustain the sun's large-scale magnetic field is actually quite low. Consider a dipole of (surface) strength $B = 10^{-3}\,\mathrm{T}$ imbedded in a sun-like sphere of radius $R = 7 \times 10^8\,\mathrm{m}$. Dimen-

sional analysis of Ampère's Law (1.4) yields

$$J \sim \frac{B}{\mu_0 R} \simeq 10^{-5}\,\mathrm{A\ m^{-2}}\ ; \tag{1.10}$$

Drift current

In the solar interior this current density is generated by a net drift speed $\mathbf{v}$ between electrons and ions, i.e., $\mathbf{J} = nq\mathbf{v}$. With an electron particle density $n \simeq 10^{29}\,\mathrm{m^{-3}}$ at the base of the solar convection zone, the required drift speed is a minuscule $|\mathbf{v}| \sim 10^{-15}\,\mathrm{m\ s^{-1}}$.

{ssec:LorentzF}

1.1.3 Backreaction: the Lorentz force

At first glance the MHD induction equation (1.5) is linear in $\mathbf{B}$, but this apparent linearity is deceptive because magnetic fields produced by dynamo action are typically not force-free, so that sufficiently strong magnetic fields will alter the inductive flow $\mathbf{u}$. This nonlinear magnetic backreaction is ultimately what limits the strength of the solar magnetic field, and thus the amplitude of the magnetic activity cycle. In the MHD limit, the Lorentz (magnetic) force per unit volume acting on the plasma is given by

{eq:Fmag1}

$$\mathbf{F} = \mathbf{J} \times \mathbf{B} \tag{1.11}$$

Lorentz force

(see §2.2 in Davidson, 2001, for an illuminating derivation). At the microscopic level the Lorentz force acts on individual charged constituents, but in a collisionally-dominated plasma the momentum so transfered to these charged constituents is very rapidly redistributed to neutrals via collisions, so that the plasma as a whole experiences a volumetric body force. It will often prove useful to decompose this force into two contributions:

{eq:Fmag2}

$$\mathbf{J} \times \mathbf{B} = \frac{1}{\mu_0}(\nabla \times \mathbf{B}) \times \mathbf{B} = \nabla\left(\frac{\mathbf{B}^2}{2\mu_0}\right) + \frac{1}{\mu_0}(\mathbf{B}\cdot\nabla)\mathbf{B}\ . \tag{1.12}$$

Magnetic pressure

Magnetic tension

The first term on the RHS is the gradient of magnetic pressure, and the second is magnetic tension.

A magnetic field is called *force-free* when $\mathbf{J} \times \mathbf{B} = 0$ everywhere in the domain under consideration. A current-free field ($\mathbf{J} = 0$) is an obvious example, in which case the magnetic field can be expressed as the gradient of a scalar potential. For specified boundary conditions, such *potential fields* represents the lowest magnetic energy state available to the system. Another class of force-free magnetic fields are those where electrical currents flow along magnetic fieldlines:

{eq:Fmag3}

$$\nabla \times \mathbf{B} = k\mathbf{B}\ , \tag{1.13}$$

where k may vary from one fieldline to the next. This expression describes a wide class of *helical fields* (see, e.g., §2.1 in Moffatt and Dormy, 2019), with k^{-1} giving the length scale on which the magnetic field is spatially structured.

Helical magnetic field

1.1.4 Energetics of dynamo action

Taking the dot product of $\mathbf{B}$ into eq. (1.5) and integrating over the volume V of the system (here the Sun) leads to the following evolution equation for the magnetic energy (E_B):

Magnetic energy

$$\frac{\mathrm{d}E_B}{\mathrm{d}t} \equiv \frac{\mathrm{d}}{\mathrm{d}t}\int_V \frac{\mathbf{B}^2}{2\mu_0}\mathrm{dV} = -\oint_{\partial \mathrm{V}} \mathbf{S}\cdot\hat{\mathbf{n}}\,\mathrm{dA} - \frac{1}{\sigma}\int_{\mathrm{V}} \mathbf{J}^2\mathrm{dV} - \int_{\mathrm{V}} \mathbf{u}\cdot(\mathbf{J}\times\mathbf{B})\mathrm{dV} \tag{1.14}$$ {eq:emag}

where $\mathbf{S} = \mu_0^{-1}\mathbf{E}\times\mathbf{B}$ [$\mathrm{W\,m^{-2}}$] is the Poynting (electromagnetic energy) flux. The associated term on the RHS of eq. (1.14) is zero for an isolated star embedded in vacuum[1]. The second term on the RHS is Ohmic dissipation, irreversibly decreasing total magnetic energy by converting it to heat. The third term is where dynamo action resides; it expresses the work per unit time done by (on) the flow against (by) the Lorentz force. This is the channel through which the kinetic energy of the flow can be converted to electromagnetic energy, a process that must take place in a manner sufficiently efficient to offset losses due to Ohmic dissipation, so that $\mathrm{d}E_B/\mathrm{d}t > 0$. This requirement is the very essence of any dynamo process, and also reveals its fundamentally nonlinear nature.

Dynamo energy conversion

1.2 Flux freezing, ideal MHD, and magnetic helicity conservation {ssec:idealMHD}

The plasma in the solar interior and atmosphere is characterized by a relatively high electrical conductivity, which leads to $\mathrm{Rm} \gg 1$ on scales ranging from convection through active regions up to the solar radius. This has crucial consequences for the dynamical interaction between flow and magnetic fields.

Go back to Faraday's Law (1.1), but now expressed in its integral form:

$$\oint_\gamma \mathbf{E}\cdot\mathrm{d}\boldsymbol{\ell} = -\frac{\partial}{\partial \mathrm{t}}\int_{\mathrm{S}} \mathbf{B}\cdot\hat{\mathbf{n}}\,\mathrm{dS}\,, \tag{1.15}$$ {eq:almost}

Here S is some arbitrarily-shaped surface with local normal unit vector $\hat{\mathbf{n}}$,

[1] This follows from $\mathbf{E}$ dropping with distance at best as r^{-2} (net electric charge) and $\mathbf{B}$ as r^{-3} (dipolar magnetic field). With the surface element dA increasing as r^2, the integrand in the surface integral on the RHS of (eq. 1.14) drops at least as r^{-3}, which guarantees that the integral vanishes as the boundary ∂V is pushed to $r \to \infty$.

bounded by the closed line γ. The LHS is the electromotive force, and the RHS is the time derivative of the magnetic flux Φ_B crossing the surface S. Assume now that S is a material surface moving with the fluid. The above expression still holds provided the partial time derivative is replaced by the Lagrangian (or material) derivative $\mathrm{D}/\mathrm{D}t \equiv \partial/\partial t + \mathbf{u}\cdot\nabla$. Moreover, the co-moving surface (and bounding line γ) being by definition at rest with respect to the moving fluid, $\mathbf{E}$ can be replaced by $\mathbf{J}/\sigma$. Thus in this Lagrangian viewpoint Eq. (1.15) becomes:

Magnetic flux

$$\frac{1}{\sigma}\oint_\gamma \mathbf{J}\cdot\mathrm{d}\boldsymbol{\ell} = -\frac{\mathrm{D}}{\mathrm{Dt}}\int_\mathrm{S}\mathbf{B}\cdot\hat{\mathbf{n}}\,\mathrm{dS}\,. \tag{1.16}$$

In the limit of infinite electrical conductivity, this expression reduces to:

{eq:alfven}

$$\frac{\mathrm{D}}{\mathrm{D}t}\int_S \mathbf{B}\cdot\hat{\mathbf{n}}\,\mathrm{dS} = 0\,. \tag{1.17}$$

This indicates that the magnetic flux threading any material surface of arbitrary shape and orientation is conserved as the surface is transported and/or deformed by the flow. This is known as *flux freezing*.

Flux freezing

The magnetic field is a solenoidal vector field, in that $\nabla\cdot\mathbf{B} = 0$; any such vector field can be expressed in terms of a vector potential $\mathbf{A}$ such that $\mathbf{B} = \nabla\times\mathbf{A}$. Stokes' theorem then permits to express eq. (1.17) in terms of the circulation Γ of $\mathbf{A}$:

{eq:alfven2}

$$\frac{\mathrm{D}\Gamma}{\mathrm{D}t} = 0\,, \qquad \Gamma = \oint_\gamma \mathbf{A}\cdot\mathrm{d}\boldsymbol{\ell}\,. \tag{1.18}$$

As depicted on Figure 1.1, Eq. (1.18) requires that a single magnetic fieldline threading any material surface bounded by the contour γ must remain "attached" to that surface as it is moved and deformed by the flow. Since the argument holds even for any infinitesimal contour enclosing any single fieldline, one must conclude that in the limit of infinite conductivity, magnetic fieldlines must move with the fluid, i.e., they are "frozen in". This is known as *Alfvén's theorem*, and is another expression of flux freezing. [2] (see also §3.1 in Moffatt and Dormy, 2019).

Alfvén's theorem

Alfvén's theorem can also be understood upon recalling that in MHD what sustains the magnetic field is the current density $\mathbf{J}$, itself associated with the very small drift speed between charged constituents of the neutral plasma (viz. §1.1.2). Infinite electrical conductivity implies that electrical charges drift through the plasma without the associated current density

[2] This is identical to the behavior of vorticity lines in inviscid fluid; in that hydrodynamical context the equivalent of (1.18) is known as Kelvin's theorem.

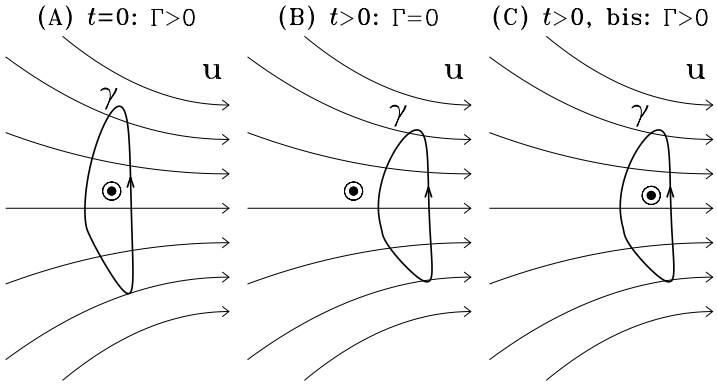

Figure 1.1 In (A), a material contour γ bounds a surface S threaded by a single magnetic fieldline pointing outside the page (indicated by a "$\odot$"). Under the right-hand rule, the circulation Γ of the associated vector potential is > 0. In (B), the contour has moved to the right but the fieldline has stayed behind; now $\Gamma = 0$, and so is the magnetic flux threading the surface bounded by γ. Equation (1.17) precludes this in the ideal MHD limit, requiring instead that the situation be as depicted in (C), where the magnetic fieldline has moved so as to remained enclosed by the material contour γ. This is flux freezing.

{fig:thalfven}

being attenuated; thus the current system $\mathbf{J}$ moves along with the bulk flow, and so does the magnetic field, as per Ampère's Law (1.4).

The case of infinite conductivity (equivalently, $\eta = 0$ or $\mathrm{Rm} \to \infty$) defines the *ideal MHD* regime. The MHD induction equation (1.5) then becomes identical to the kinematic theorem describing the advection of a line element by a flow $\mathbf{u}$, implying again that magnetic fieldlines move with the fluid (see, e.g., Davidson 2001, §2.7.4). The consequent ability of the fluid flow to bend and stretch magnetic fieldlines, in the very high Rm regime relevant to the solar plasma, is at the heart of the MHD induction mechanism.

Ideal MHD

This has far-reaching consequences because flux freezing also implies that magnetic fieldlines cannot break or cross one another, which poses a strong topological constraint on the field's spatiotemporal evolution. This can be quantified through magnetic helicity, a global topological measure of linkage between magnetic flux systems threading a given volume **?**Berger (1999); Pevtsov et al. (2014):

$$\mathcal{H}_B = \int_V \mathbf{A} \cdot \mathbf{B} \mathrm{dV}, \tag{1.19}$$

Magnetic helicity

{eq:maghel}

where again the vector potential $\mathbf{A}$ is such that $\mathbf{B} = \nabla \times \mathbf{A}$. In a closed system, i.e. without helicity flux through its boundaries, magnetic helicity

can be shown to evolve according to (see Brandenburg and Subramanian, 2005; **?**, chap. 3):

{eq:totalhel}
$$\frac{\mathrm{d}}{\mathrm{d}t}\int \mathbf{A}\cdot\mathbf{B}\mathrm{d}V = -2\mu_0\eta\int \mathbf{J}\cdot\mathbf{B}\mathrm{d}V\ , \tag{1.20}$$

In ideal limit $\eta \to 0$, which is the relevant limit for dynamo action in the interior of the sun and stars, the RHS vanishes and eq. (1.20) then indicates that total helicity must be conserved, or at best vary on the long diffusive timescale τ_η. Conservation of magnetic helicity thus puts a strong constraint on the high-Rm amplification of any magnetic field that carries a net helicity, which is certainly the case with the large-scale solar magnetic field.

Helicity conservation

{sec:BSources}
1.3 Mechanisms of magnetic field generation

In its conceptually simplest form, the dynamo problem consists in finding a flow $\mathbf{u}$ which, when inserted in the MHD induction equation (1.5), leads to amplification of and sustenance of $\mathbf{B}$ against Ohmic dissipation. From this point of view our prospects are quite good, because vigorous flows abound in the sun. Thermally-driven turbulent convection transports the bulk of the solar luminosity in the outer 30% of the sun's radius. This same turbulent convection also generates Reynolds stressess driving inverse cascades that power large-scale flows, notably *differential rotation* and *meridional circulation* (see, e.g. Miesch and Toomre, 2009). Energetically, solar convection and differential rotation are the primary contributors to $\mathbf{u}$ in eqs. (1.5) and (1.14).

{ssec:drshear}
1.3.1 Shearing by differential rotation

Shearing of a large-scale poloidal magnetic field by differential rotation turns out to be a key ingredient in nearly all solar cycle models considered in the remainder of this book, so we first examine this induction mechanism.

Working in spherical polar coordinates (r,θ,ϕ), we consider the shearing of an axisymmetric ($\partial/\partial\phi \equiv 0$) poloidal magnetic field (component contained in meridional planes) by a steady differential rotation (an axisymmetric zonal flow):

{eq:shear1a}
$$\mathbf{u} = \varpi\,\Omega(r,\theta)\hat{\mathbf{e}}_\phi\ . \tag{1.21}$$

{eq:shear1b}
$$\mathbf{B}_p \equiv B_r(r,\theta)\hat{\mathbf{e}}_r + B_\theta(r,\theta)\hat{\mathbf{e}}_\theta\ . \tag{1.22}$$

where $\varpi \equiv r\sin\theta$ is the cylindrical radius. Under this very simple configuration, neglecting Ohmic dissipation, and for a purely poloidal magnetic field

at $t = 0$, the ϕ-component of the induction equation (1.5) integrates to

{eq:shear2}
$$B_\phi(r,\theta,t) = \varpi(\mathbf{B}_p \cdot \nabla\Omega)\, t \ , \tag{1.23}$$

i.e., at any point in the meridional $[r,\theta]$ plane, the toroidal magnetic component grows linearly in time, at a rate proportional to the local poloidal field strength and magnitude of the rotational shear.

Figure 1.2 illustrated this shearing process, for the case of a dipolar large-scale magnetic field (red fieldlines on panel A) being sheared by a solar internal rotation profile displayed on panel (A) as green isocontours of angular velocity $\Omega(r,\theta)$. Such a profile is characterized by a more rapidly rotating equator and slowly rotating pole through the convective envelope ($0.7 \leq r/R \leq 1$), matching onto a rigily rotating radiative core across a thin rotational shear layer called the *tachocline* (Brown et al., 1989; Spiegel and Zahn, 1992; Howe, 2009), straddling the core-envelope interface (dashed circular arcs on all panels of Fig. 1.2). The angular velocity also drops significantly in the subsurface layers, generating a layer of strong negative radial shear ($\partial\Omega/\partial r < 0$) from the equator up to $\sim 60^\circ$ latitude. Panel (B) is a color rendering of the toroidal magnetic component produced by this shearing process. The strongest toroidal fields are produced in regions of strong shear where poloidal fieldline are most closely aligned with $\nabla\Omega$, as expressed by eq. (1.23). For the solar-like differential rotation profile used here, strong toroidal fields are produced in the tachocline and subsurface shear layer through the agency of radial shear, and at mid-latitudes within the convection zone primarily via the latitudinal shear.

Solar differental rotation

Tachocline

Surface shear layer

One can readily verify that a solar-like 10^{-3} T poloidal field, when subjected to a solar-like pole-to-equator angular velocity contrast $+10^{-6}\,\mathrm{rad\,s^{-1}}$ induces in 10 yr a toroidal component of strength ~ 0.3 T. This is commensurate with estimates of the strength of the sunspot-forming internal solar magnetic field (Fan, 2009, and references therein). Because the latitudinal shear changes sign across the equator, the induced toroidal field will also be antisymmetric about the equator, which is the parity inferred from Hale's polarity Laws.

REF to other chapter

With the toroidal component growing linearly with time according to eq. (1.23), so will the Lorentz force. For the setup considered here its component in the ϕ-direction is given by:

{eq:shear3}
$$F_\phi(r,\theta,t) = \frac{t}{\mu_0 \varpi}\mathbf{B}_p \cdot \nabla[\varpi B_\phi(r,\theta,t)] \ . \tag{1.24}$$

This zonal component of the Lorentz force is illustrated on Fig. 1.2C. Careful comparison with panel (A) reveals the Lorentz force acts here in a direction

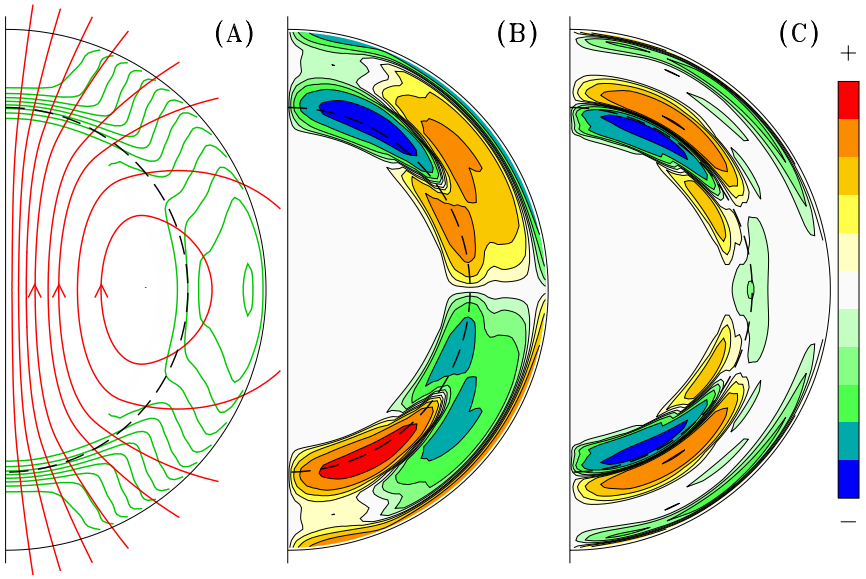

Figure 1.2 Shearing of an axisymmetric large-scale poloidal magnetic field (red fieldlines on panel A) by the solar differential rotation (green isocontours in A). The resulting toroidal magnetic component on panel B is antisymmetric about the equatorial plane, and peaks here in the tachocline, where rotational shear is strongest. The associated Lorentz force on panel C always opposes the shearing flow, as is required for energy transfer from the flow to the magnetic field. The dashed circular arc indicates the base of the convective envelope. {fig:shearpol}

such as to reduce the rotational shear. This is in fact required by eq. (1.14) if energy is to be extracted from the flow, to supply the magnetic energy associated with the growth of the toroidal magnetic component. This is a general, robust result, which is not at all restricted to the flow/field configuration considered here.

Setting eq. (1.24) equal to zonal acceleration per unit mass, dimensional analysis indicates that the Lorentz force will backreact on differential rotation on a dynamical timescale given by:

$$\tau_\Omega = \frac{\mu_0 \rho L^2 \Omega}{B_p B_\phi} \ . \tag{1.25}$$

Using the numerical values $B_\phi \sim 1\,\mathrm{T}$ and $\rho \sim 10\,\mathrm{kg\,m^{-3}}$ for the outer half of the solar convection zone yields $\tau_\Omega \sim 10^3\,\mathrm{yr}$; and a $\sim 1\%$ variation in Ω,

commensurate with observed solar torsional oscillations (Howe, 2009), can be generated in $\sim 10\,\mathrm{yr}$.

1.3.2 Cowling's theorem {ssec:cowling}

Rotational shearing of a steady ($\partial/\partial t \equiv 0$) axisymmetric ($\partial/\partial\phi \equiv 0$) poloidal magnetic field by steady differential rotation, as we just considered, obviously cannot produce polarity reversals. Less obvious but even more important is the fact that this setup in itself, cannot sustain the magnetic field against Ohmic dissipation over timescales of the order of the magnetic diffusion time (eq. (1.9)). To understand why consider the following representation of an axisymmetric magnetic field, whereby its poloidal component is defined in terms of a toroidal vector potential $\mathbf{A} = A(r,\theta)\hat{\mathbf{e}}_\phi$:

$$\mathbf{B}(r,\theta,t) = \underbrace{\nabla\times(A(r,\theta,t)\hat{\mathbf{e}}_\phi)}_{\text{poloidal}} + \underbrace{B(r,\theta,t)\hat{\mathbf{e}}_\phi}_{\text{toroidal}} \,. \tag{1.26}$$ {eq:Baxi}

This ensures $\nabla\cdot\mathbf{B} = 0$ for any axisymmetric magnetic field so constructed. Again retaining only the contribution of differential rotation to the large-scale flow (viz. eq. (1.21)), substitution of eq. (1.26) into the induction equation allows to separate the latter into the following pair of evolution equations for A and B:

$$\frac{\partial A}{\partial t} = \eta\left(\nabla^2 - \frac{1}{\varpi^2}\right)A \,, \tag{1.27}$$ {eq:cowa}

$$\frac{\partial B}{\partial t} = \eta\left(\nabla^2 - \frac{1}{\varpi^2}\right)B + \varpi(\nabla\times(A\hat{\mathbf{e}}_\phi))\cdot\nabla\Omega \,, \tag{1.28}$$ {eq:cowb}

where the magnetic diffusivity η is assumed constant. The second term on the RHS of (1.28) acts as a source term for B, proportional to A; however, no such source is present on the RHS of eq. (1.27). As a consequence, the latter can only resistively decay on the diffusive timescale (1.9). Once A has vanished, the source term on the RHS of eq. (1.28) also vanishes, and from that point on B will also decay on the resistive timescale. This is the essence of *Cowling's theorem*: an axisymmetric flow cannot support an axisymmetric magnetic field against Ohmic dissipation. The apparently unbounded linear growth of the toroidal magnetic field obtained previously (eq. (1.23)) results from having assumed a steady poloidal component; as a solution of the induction equation, this is therefore only (approximately) valid for times much shorter than the diffusion time (1.9). In itself, the flow/field system of §1.3.1 is not a dynamo.

Escape from Cowling's theorem must therefore involve departures from axisymmetry. In the solar case salvation can be found in turbulent convection, but at the price of facing the wide disparity of scales and dynamical intricacies characterizing MHD turbulence at high fluid and magnetic Reynolds numbers.

{ssec:fastdyn}

1.3.3 Small-scale flows and dynamos

The structure of the inductive term $\nabla \times (\mathbf{u} \times \mathbf{B})$ in the MHD induction equation (1.5) certainly suggests that magnetic fields are produced on a spatial scale commensurate with that of the flow $\mathbf{u}$. In what follows, fluid dynamos generating magnetic structures on the scale of the inductive flow (or smaller) are referred to as *small-scale dynamos*.

Small-scale dynamo

Working in the ideal MHD limit $\eta \to 0$, it will prove useful to first recast the induction equation in the form:

{eq:inductexpand}

$$\underbrace{\left(\frac{\partial}{\partial t} + \mathbf{u}\cdot\nabla\right)}_{\text{advection}}\mathbf{B} = \underbrace{(\mathbf{B}\cdot\nabla)\mathbf{u}}_{\text{shearing}} - \underbrace{\mathbf{B}(\nabla\cdot\mathbf{u})}_{\text{compression}} \ . \tag{1.29}$$

The advection operator on the LHS is just the Lagrangian derivative, and captures the bulk transport of $\mathbf{B}$ by the flow $\mathbf{u}$, without deformation of amplification. The shearing term we encountered already on the RHS of Eq. (1.23). It can obviously amplify $\mathbf{B}$, as seen already in §1.3.1. The compression term can also act to amplify $\mathbf{B}$; for very subsonic flows the mass conservation constraint is well approximated by $\nabla\cdot(\rho\mathbf{u}) \simeq 0$, so that $\nabla\cdot\mathbf{u} = -\mathbf{u}\cdot\nabla(\log\rho)$. In the strongly stratified outer convection zone and photosphere, strong field amplification can take place via this term, with the scale height of the stratification now imprinting itself on the vertical structure of the induced field.

Both terms on the RHS of (1.29) are linear in $\mathbf{B}$ and proportional to derivatives of $\mathbf{u}$; Assuming again that $\mathbf{u}$ is steady, the required mathematical ingredients for exponential growth of the magnetic field are clearly present in Eq. (1.29). How this pans out in a real flow, however, turns out to be anything but simple.

Consider first the very simple situation depicted in Figure 1.3. A bundle of horizontal magnetic fieldline is threading a cylindrical volume element of plasma. The term "magnetic flux tube" will be used to characterize this highly idealized magnetized plasma structure. The gray lines are streamlines of a steady, incompressible flow including a stagnation point, as indicated by the gray dot labeled P. While the flow pushes the tube vertically

Magnetic flux tube

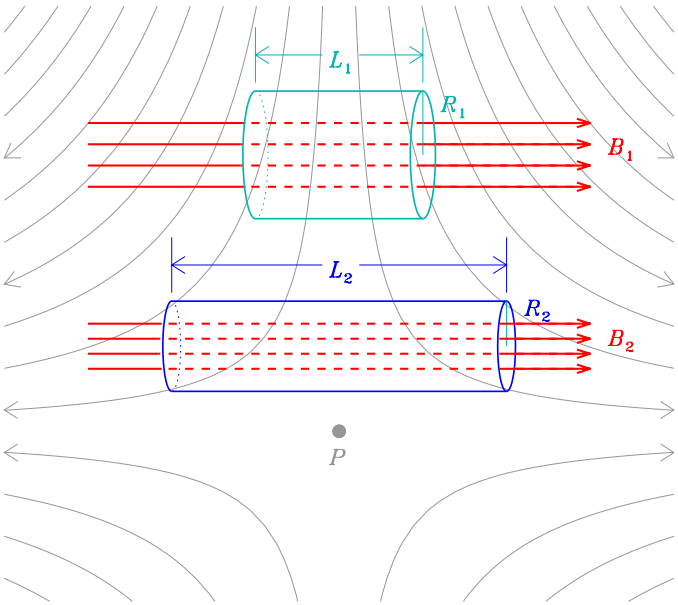

Figure 1.3 Stretching of a magnetic flux tube in the vicinity of a hyperbolic stagnation point (in gray, labeled P). Here a cylinder of incompressible fluid threaded by a magnetic field (in red) parallel to its axis is inexorably stretched horizontally as it is displaced downwards towards the stagnation point, leading to amplification of the magnetic field intensity through flux conservation (see text). Flow streamlines are drawn in gray.

{fig:stagpoint}

downwards (advection term in Eq. (1.29)), flow gradients stretch the tube horizontally (shearing term in Eq. 1.29), here from length L_1 (in light blue) to length L_2 (dark blue) at some later time. The flow being incompressible, mass conservation requires that the radius R of the tube's cross-section decreases as $R_2/R_1 = \sqrt{L_2/L_1}$. Under flux freezing, the (uniform) magnetic field strength within the tube must then increase as $B_2/B_1 = L_2/L_1$, i.e., in direct proportion to the amount of stretching. Magnetic energy also increases, as $(L_2/L_1)^2$, ultimately in response to the work done by the vertical component of the flow on the magnetic pressure gradient, pointing radially outwards at the tube's boundary. However, here no new magnetic flux is generated; indeed, field amplification is a direct consequence of magnetic flux conservation as the tube's section decreases.

The bulk downwards advection of the tube stops once it reaches the stag-

nation point; but stretching and compression do not. Near the stagnation point, $u_x \propto x$ and $u_y \propto -y$, which leads to exponential stretching in x and exponential compression in y. As a consequence, the radius R of the tube inexorably decreases with time, until Ohmic dissipation can operate on a timescale $\tau_\eta = R^2/\eta$ commensurate with the stretching timescale $\tau_u = R/u$. Once this $\mathrm{Rm} = 1$ stage is reached, resistive decay of the magnetic field sets in. The smaller the magnetic diffusivity η, the longer it will take to reach this dissipation radius; but this will always happen here, no matter how small η might be, since τ_η scales as R^2, while τ_u scales linearly with R. One can but conclude that this flow is not a proper dynamo.

Consider now the situation depicted on Figure 1.4. Working still under flux freezing, a closed, circular magnetic flux tube of unit radius and cross-section a initially positioned in the xy plane (panel a) is gradually tilted out of that plane (in b) by an incompressible, now time-dependent flow. In addition to tilting the loop, this flow also pushes one sector of the tube inwards (b→c), thus introducing a twist and leading to the formation of a second loop where the magnetic field orientation is the same as that of the original flux ring (c→e). At the end of this process (panel f), the original ring-shaped magnetic flux tube has been stretched into two loops of unit radius, pressed against one another in the xy plane; magnetic fieldlines within the two loops are all parallel to one another, except at a single crossing point (here the dark blue to dark red transition).

It is clear from Fig. 1.4a→f that the total length of the loop has doubled, with mass conservation again imposing a decrease of the cross-section by a factor of two; as before, magnetic flux conservation leads to a corresponding increase in field strength also by a factor of two. However, now the total magnetic flux across a given cross-section of the two-loop structure has also doubled. This so-called Stretch-Twist-Fold (STF) sequence exemplifies the process of *constructive folding*. The twisting motion is essential here; if the loop were only stretched radially outward and folder over (say) without a twist, magnetic fieldlines with each loop would point in opposite directions, and add up to zero net magnetic flux, and the strong magnetic field gradients so produced would favor dissipation. This would then be an instance of *destructive folding*.

Stretch-Twist-Fold Constructive folding

If the process is now repeated starting from the configuration in (f), after another such stretch-twist-fold sequence there will now be four unit-radius flux rings stacked together. After n such sequences, the total length of the tube, the number of stacked loops, the field strength within the tube, and the total flux in a cross-section of the bundle, all have increased by a factor 2^n. Mass conservation, in turn, requires the section of each loop to have

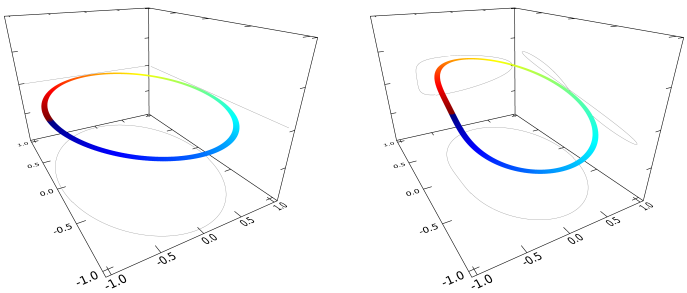

(a)

(b)

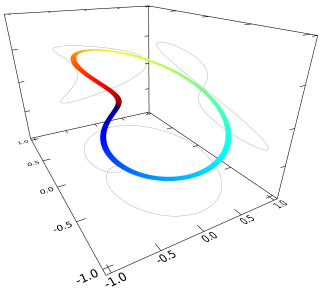

(c)

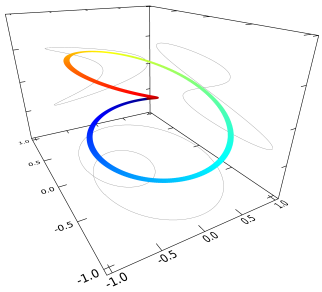

(d)

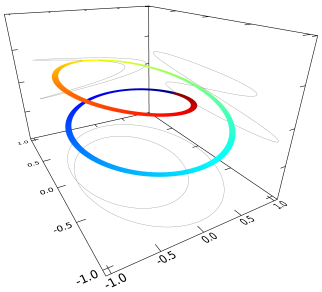

(e)

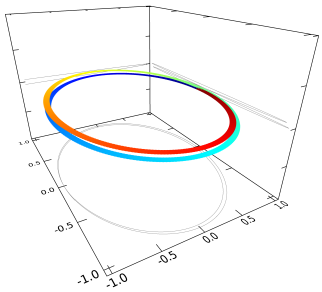

(f)

Figure 1.4 Stretching, twisting and folding of an initially circular magnetic flux ring. The gray lines are "shadows" of the tube projected on the three coordinate planes, to help visualize the 3D distorsion of the tube with time. The end product is a stack of two flux rings of twice the field strength of the original ring, and jointly adding up to twice the magnetic flux (see text). This is the celebrated Stretch-Twist-Fold dynamo of Vainshtein & Zel'dovich.

{fig:stf}

decreased as 2^{-n}. Assume now that the 2^n loops, each of section $a \times 2^{-n}$, but with their magnetic fields all parallel, can coalesce into a single loop while conserving mass and magnetic flux; this new single loop is back to the original cross-section a, while still carrying 2^n times the magnetic flux of the initial ring. This therefore avoids the inexorable decrease of length scale that ultimately made it impossible for the stagnation point flow of Fig. 1.3 to act as a bona fide dynamo.

If now we interpret the iteration variable n as some discretization of time t, the 2^n increase of the magnetic field strength is equivalent to an exponential growth of the form

$$\frac{B(t)}{B(0)} = \exp(t \log 2) \ . \tag{1.30}$$

The flow driving the STF sequence of Fig. 1.4 is thus a dynamo. The increase of magnetic energy results from the work done by the flow against magnetic tension in deforming and stretching the flux ring. It is deemed a *fast dynamo* because the growth rate of the magnetic field, here equal to log 2, is independent of magnetic diffusivity, indicating that this dynamo can operate in the $\mathrm{Rm} \to \infty$ regime[3]. Other types of dynamos to be encountered shortly, in contrast, are characterized by growth rates that tend to zero as $\mathrm{Rm} \to \infty$; those are characterized as *slow dynamos*.

Fast dynamo

Slow dynamo

Considerable efforts have been made towards understanding which flow properties are conducive to dynamo action, whether fast or slow. The topic is very comprehensively covered in Childress and Gilbert (1995), Moffatt and Dormy (2019), and at a more elementary level in chapter 2 of Charbonneau (2013). The results most pertinent to the foregoing discussion can be summarized as follows:

1. Fast dynamo action requires the inductive flow to have chaotic streamlines;
2. Whether fast or slow, in the high-Rm regime small-scale dynamos tend to produce magnetic structures that are spatiotemporally intermittent, and with typical length scales $\mathrm{Rm}^{-1/2}\ell$, where ℓ is the characteristic spatial scale of the inductive flow;
3. Small-scale dynamos can produce a lot of magnetic field, but very little net magnetic flux on scales significantly larger than the flow.

[3] Strictly speaking, the STF dynamo requires magnetic dissipation to ensure the coalescence of the 2^n flux loops produced after n STF steps; otherwise, because the section of each loop decreases as 2^{-n}, dissipation would eventually set in even for very large Rm, exactly as it did for the straight flux tube of Fig. 1.3. Dissipation is also required to offset the buildup of magnetic helicity that takes place at the point of crossing of the loops during coalescence. See §10.1 in Moffatt and Dormy (2019) for more on these (and other) subtleties associated with the STF dynamo.

These results were established for the most part using artificial flows, either assumed steady of with an imposed time-dependency or mechanical forcing, but have been found to carry over to more realistic situations in which the dynamical backreaction of the Lorentz force on the inductive flow is included self-consistently. Local area, high resolution MHD numerical simulations of solar convection, with ever increasing resolution and physical realism, have amply demonstrated its ability to achieve dynamo action and sustain equipartition-strength magnetic fields (see, e.g. Cattaneo, 1999; Stein and Nordlund, 2006; Vögler and Schüssler, 2007; **?**; Rempel, 2014; Hotta et al., 2015, and references therein; and for a comprehensive review, Stein 2012).

Figures 1.5 and 1.6 shows surface snapshots of a high resolution MURaM radiative MHD simulation of thermally-driven convection, taken from Rempel (2014). Figure 1.5 is a continuum intensity image, with granules showing up as broad brighter areas, separated by a network of darker narrow downflow lanes of colder fluid. Figure 1.6 is a grayscale rendition of the surface radial magnetic field. On both Figures the colored contours delineate regions where the radial surface magnetic field exceeds 1kG in strength. This simulation is a restart at twice the spatial resolution of case O16bM in Rempel (2014), that simulation itself initialized from a weak ($\sim 10^{-3}$ G) vertical magnetic field of strength varying randomly in the horizontal. The two snapshopts displayed here are extracted from the statistically stationary, saturated phase of the simulation.

In this simulation, small-scale dynamo action amplifies the magnetic field by stretching and shearing throughout the convecting fluid layers, tapping into the energy of convective fluid motions. The spatiotemporal evolution of the surface magnetic field, however, is strongly influenced by convective granulation and radiative cooling in strong magnetic flux concentrations accumulating in intergranular lanes, leading to further field amplification and spatial organization on granular scale.

The photospheric snapshot of Figure 1.5 is a 3.2×3.2 Mn shapshot of this 25×25 Mm simulation, and shows how warm (bright) fluid rises in the center of granules, and cools as it spreads out towards the intergranular lanes, where it sinks back to the interior. In doing so, the (relatively) weak magnetic fields brought to the surface by convection (advection term in eq. (1.29) is swept into intergranular lanes, where it is amplified (compression term in Eq. (1.29)). Once in downflow lanes, the magnetic field is further amplified by shearing at the downflow's edges (Rempel, 2018), despite the small horizontal length scale favoring dissipation. Under the joint action of advection and dissipation, the field eventually coalesces into buoyant, long-

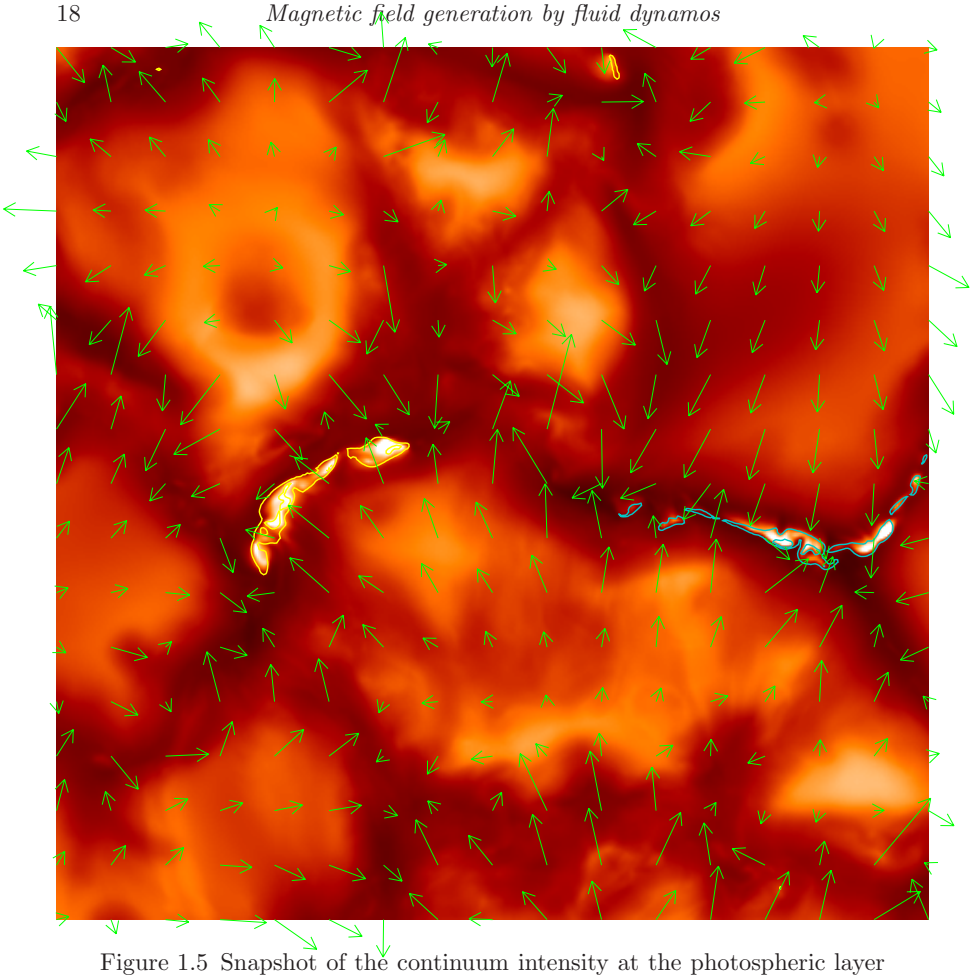

Figure 1.5 Snapshot of the continuum intensity at the photospheric layer in a local area MHD numerical simulation of solar convection. Cooler (warmer) fluid is rendered in darker (lighter) shade of orange. This is a closeup covering 3.2×3.2 Mm, with an horizontal resolution of 8 km. The green arrows depict the horizontal flow components at a subset of grid points. The brighter diffuse patches are granules, with a typical horizontal size of ~ 1 Mm. The colored contours delineate regions having a vertical magnetic field strength $|B_z| \geq 1$ kG, yellow (blue) indicating positive (negative) B_z. Figure generated from numerical data kindly provided by M. Rempel. {fig:muram}

lived compact and vertically-oriented magnetic flux concentrations exceeding energy equipartition with fluid motions; there are highlighted by yellow and blue contours on Figs. 1.5 and 1.6,

Examination of the vertical field distribution displayed on Fig. 1.6 gives

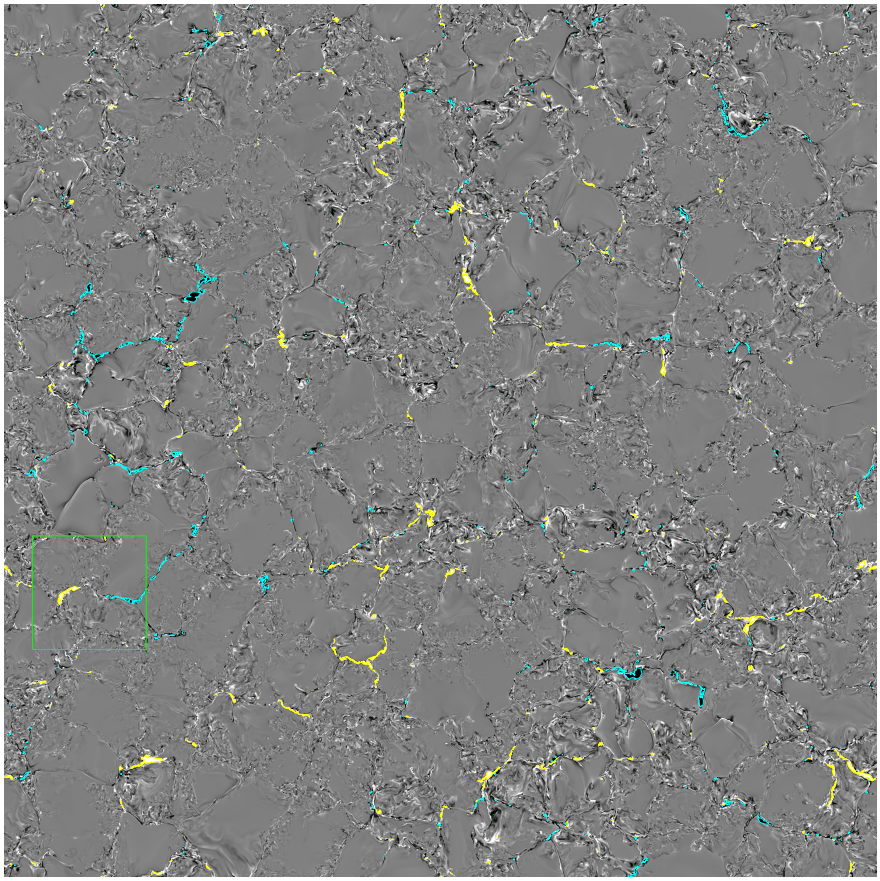

Figure 1.6 Snapshot of the vertical magnetic field at the same simulation time as the continuum image of Fig. 1.5, but now over the full $25 \times 25\,\mathrm{Mm}$ horizontal domain size. The spatial extent of the closeup of Fig. 1.5 is indicated by the green square. The grayscale rendering spans the range $-0.5\,\mathrm{kG} \leq B_z \leq +0.5\,\mathrm{kG}$, from black to white. The colored contours delinate regions having a vertical magnetic field $|B_z| \geq 1kG$, yellow (blue) indicating positive (negative) B_z. Figure generated from numerical data kindly provided by M. Rempel. {fig:muram2}

the impression that the vertical magnetic field displays an even mixture of negative and positive polarity. This visual impression is confirmed by computing density histogram of nodal magnetic field values, a displayed on Fig. 1.7 for the vertical field B_z (red) and the horizontal component B_y (blue). Both density histograms are symmetric about zero, indicating that

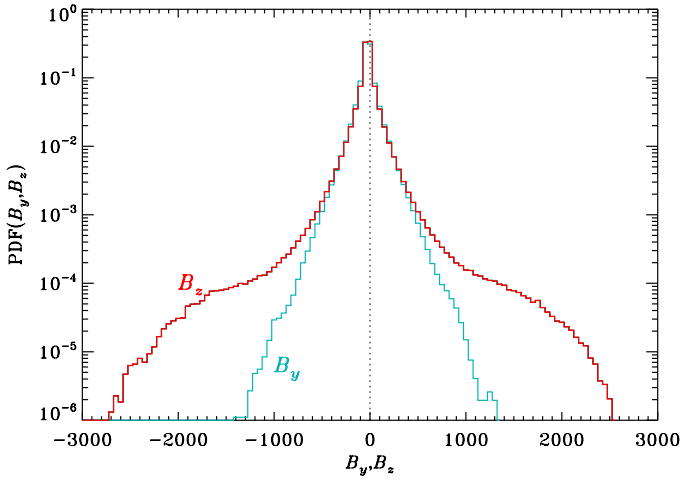

Figure 1.7 Probability density function for the vertical magnetic field values in the snapshot of Fig. 1.6 (red), and also for the B_y horizontal component (blue). Both PDFs are symmetric about zero, indicating zero magnetic flux on the scale of the simulation domain. Figure generated from numerical data kindly provided by M. Rempel.

{fig:muram_bh}

no net magnetic flux is produced on spatial scales larger than granular, despite strong local field amplification taking place on subgranular scales. The extended high field strength tails in the B_z density histograms, absent for the horizontal component B_y, reflect the aforementioned buildup of super-equipartition concentrations of vertical magnetic field in intergranular lanes. Similar high resolution local area simulations in which significant magnetic flux is injected at the lower boundary have also demonstrate the ability of convection to build up photospheric magnetic flux concentrations on scales much larger than intergranular, akin to pores and sunspots (see, e.g. Cheung et al., 2010; Stein and Nordlund, 2012; Cheung and Isobe, 2014; Rempel and Cheung, 2014, for a representative sample of such simulations)

Fluid dynamos generating magnetic structures on the scale of the inductive flow (or smaller) are referred to as *small-scale dynamos*. The MURaM MHD convection simulation of Fig. 1.5 is a dynamo of this variety, and does provide a convincing explanatory framework for the origin of the strong and spatiotemporally intermittent magnetic field concentrations observed in the solar photosphere. In contrast, the magnetic field component associated with the solar 11-yr activity cycle is structured on scales much larger than convection, commensurate in fact with the solar radius, and is character-

ized by a significant amount of net magnetic flux on those scales, persisting over timecales much longer than the convective turnover time. How, then, can turbulent solar convection, with typical scales of order 10^5–10^7 m and 10^3–10^6 s, induce and sustain against destructive folding and dissipation a spatiotemporally coherent magnetic component with scales of order 10^9 m and 10^8 s?

Fluids dynamos achieving the amplification and sustenance of such large-scale magnetic fields are known as *large-scale dynamos*. They can still be powered by small-scale fluid motions such as thermally-driven convection, provided some physical effect(s) can drive self-organization of the magnetic field on those larger scales (see Tobias et al., 2011, for more on this point). This is the topic to which we now turn.

Large-scale dynamo

1.3.4 Mean-field electrodynamics and the α-effect {ssec:alpha}

It is an observed fact that solar convection is characterized by spatial scales much smaller that the solar radius; and that the magnetic field associated with the solar activity cycle is spatially organized on the much larger global scale of the sun. This *scale separation* is at the core of *mean-field electrodynamic*, an approach allowing to capture statistically the inductive effect of a small-scale turbulent flow on the large-scale magnetic component.

The first step is to separate the total flow and magnetic field into large-scale and small-scale contributions:

Scale separation

$$\mathbf{B} = \langle \mathbf{B} \rangle + \mathbf{b}' \ , \qquad \mathbf{u} = \langle \mathbf{U} \rangle + \mathbf{u}' \ , \tag{1.31}$$ {eq:scalesep}

where the angular brackets denote an averaging over an intermediate length scale, sufficiently large so that $\langle \mathbf{u}' \rangle = 0$ and $\langle \mathbf{b}' \rangle = 0$. This is not a linearization, as no assumptions are being made regarding the magnitude of $\mathbf{u}'$ versus $\langle \mathbf{U} \rangle$, or $\mathbf{b}'$ vs $\langle \mathbf{B} \rangle$. Inserting eq. (1.31) into the MHD induction equation (1.5) and averaging leads to the *mean-field induction equation*:

$$\frac{\partial \langle \mathbf{B} \rangle}{\partial t} = \nabla \times \left(\langle \mathbf{U} \rangle \times \langle \mathbf{B} \rangle + \boldsymbol{\xi} - \eta \nabla \times \langle \mathbf{B} \rangle \right) \ , \tag{1.32}$$ {eq:mfmhd}

where

Mean emf

$$\boldsymbol{\xi} = \langle \mathbf{u}' \times \mathbf{b}' \rangle \tag{1.33}$$ {eq:emf}

is the *mean electromotive force* (hereafter emf) produced by correlated fluctuations of the flow and field at small scales. The key point is that this emf can act as a source term for $\langle \mathbf{B} \rangle$, because it will not necessarily average

to zero, even though $\mathbf{u}'$ and $\mathbf{b}'$ individually do[4] If eqs. (1.31) are inserted into the MHD induction equation, without averaging, but now subtracting eq. (1.32), one obtains an evolutionary equation for the small scale field:

{eq:ffmhd}
$$\frac{\partial \mathbf{b}'}{\partial t} = \nabla \times (\langle \mathbf{U} \rangle \times \mathbf{b}' + \mathbf{u}' \times \langle \mathbf{B} \rangle + \mathbf{u}' \times \mathbf{b}' - \boldsymbol{\xi} - \eta \nabla \times \mathbf{b}') \ . \tag{1.34}$$

Formally solving eqs. (1.32) and (1.34) as a coupled system is not a desirable avenue here, as the whole aim of the mean-field approach is to avoid having to deal explicitly with the small scales. Consider instead the mathematical nature of the coupling between eqs. (1.32) and (1.34); for $\mathbf{u}'$ considered given, eq. (1.34) is linear in $\mathbf{b}'$, except for a source term $(\mathbf{u}' \times \langle \mathbf{B} \rangle)$ linear in $\langle \mathbf{B} \rangle$; similarly, with $\langle \mathbf{U} \rangle$ and $\mathbf{u}'$ given, eq. (1.32) is linear in $\langle \mathbf{B} \rangle$, except for $\boldsymbol{\xi}$ providing a source term linear in $\mathbf{b}'$. It follows that the mean emf can be expressed as a linear (tensorial) development in terms of the large-scale magnetic field:

{eq:emfab}
$$\mathcal{E}_i = a_{ij} \langle B \rangle_j + b_{ijk} \frac{\partial \langle B \rangle_j}{\partial x_k} + ... \ , \tag{1.35}$$

where the tensors $\mathbf{a}$, $\mathbf{b}$, etc, depend on the properties of the flow, but cannot depend on $\langle \mathbf{B} \rangle$. It is physically illuminating to explicitly separate the symmetric and antisymmetric parts of these tensors, so that the emf becomes

{eq:abexpand}
$$\boldsymbol{\xi} = \boldsymbol{\alpha} \cdot \langle \mathbf{B} \rangle + \boldsymbol{\gamma} \times \langle \mathbf{B} \rangle - \boldsymbol{\beta} \cdot (\nabla \times \langle \mathbf{B} \rangle) + ... \tag{1.36}$$

The symmetric rank-2 tensor $\boldsymbol{\alpha}$ is just the symmetric part of a_{ij}, the pseudo-velocity $\boldsymbol{\gamma}$ collects its three independent antisymmetric components, and the rank-2 tensor $\boldsymbol{\beta}$ collects the antisymmetric parts of b_{ijk}:

{eq:alphabetagamma}
$$\alpha_{ij} = \frac{1}{2}(a_{ij} + a_{ji}) \ , \tag{1.37}$$

$$\gamma_k = -\frac{1}{2} \epsilon_{kij} a_{ij} \ , \tag{1.38}$$

$$\beta_{ij} = \frac{1}{4}(\epsilon_{ikl} b_{jkl} + \epsilon_{jkl} b_{ikl}) \ , \tag{1.39}$$

(see Krause and Rädler, 1980; Schrinner et al., 2007, for further details). These three quantities capture the physical effects most often invoked in constructing mean-field dynamo models of the solar cycle, and in principle can be computed if the statistical properties of the turbulent flow and field are known. For perfectly homogeneous, isotropic turbulence, one expects

$$\alpha_{ij} = \alpha \delta_{ij} \ , \tag{1.40}$$

[4] This mean electromotive force is entirely analogous to the Reynolds stresses appearing in the Navier-Stokes unmagnetized fluid equations upon introducing scale separation and averaging.

$$\gamma_k = 0 \ , \tag{1.41}$$

$$\beta_{ij} = \beta\delta_{ij} \ , \tag{1.42}$$

where δ_{ij} is the usual Kronecker delta. Truncating eq. (1.35) after the second term and substituting in the mean-field induction equation (1.32) then yields:

$$\frac{\partial\langle\mathbf{B}\rangle}{\partial t} = \nabla\times\left(\langle\mathbf{U}\rangle\times\langle\mathbf{B}\rangle + \alpha\langle\mathbf{B}\rangle - (\eta+\beta)\nabla\times\langle\mathbf{B}\rangle\right) \ . \tag{1.43}$$ {eq:mfmhd2}

The α-term now emerges as a (turbulent) electromotive force aligned with the mean-magnetic field, in contrast to the conventional motional emf $\propto \langle\mathbf{U}\rangle\times\langle\mathbf{B}\rangle$ which is perpendicular to $\langle\mathbf{B}\rangle$. This contribution to the total turbulent emf, crucial in many dynamo models discussed further below, is known as the α-*effect*, and is non-zero for flows lacking reflection symmetry.

α-effect

The second term in the expansion (1.35), reduced to the β-term in (1.36), makes an an additive contribution to the magnetic diffusivity η, and can thus be interpreted as *turbulent diffusion* of $\langle\mathbf{B}\rangle$. The α- and β-effects in eq. (1.43) embody, respectively, constructive and destructive folding of the mean-magnetic field by the small-scale turbulent flow (see Fig. 1.8). In other words, turbulence may provide a mean-electromotive force acting as a source for the mean-magnetic field, but it will also inevitably generate enhanced dissipation of that same mean magnetic field. No free lunch !

turbulent diffusivity

Approximate expressions for α, β and $\boldsymbol{\gamma}$ can be obtained for turbulence that is midly inhomogeneous and anisotropic, as would be expected in the presence fo stratification and rotation. Tractable formulations are restricted in a few specific physical regimes: low magnetic Reynolds number, turbulence with short coherence time, or strong mean magnetic field. In all cases this amounts to the large-scale mean magnetic field suffering little deformation by the small-scale flow, as on Fig. 1.8A. In these regimes it can be shown that:

$$\alpha = -\frac{\tau_c}{3}\langle\mathbf{u}'\cdot(\nabla\times\mathbf{u}')\rangle \ , \tag{1.44}$$ {eq:socaalpha}

$$\boldsymbol{\gamma} = -\frac{\tau}{6}\nabla\langle(\mathbf{u}')^2\rangle \ , \tag{1.45}$$ {eq:socagamma}

$$\beta = \frac{\tau_c}{3}\langle(\mathbf{u}')^2\rangle \ . \tag{1.46}$$ {eq:socabeta}

(see, e.g., Ossendrijver, 2003; Brandenburg and Subramanian, 2005; **?**, chap. 3). Order-of-magnitude estimates for the middle of the solar convection zone using $|\mathbf{u}'| \sim 10\,\mathrm{m\,s^{-1}}$ and $\tau_c \sim 1\,$month lead to $\beta \sim 10^8\,\mathrm{m^2 s^{-1}}$, and α and $|\boldsymbol{\gamma}|$ both in the $\mathrm{m\,s^{-1}}$ range.

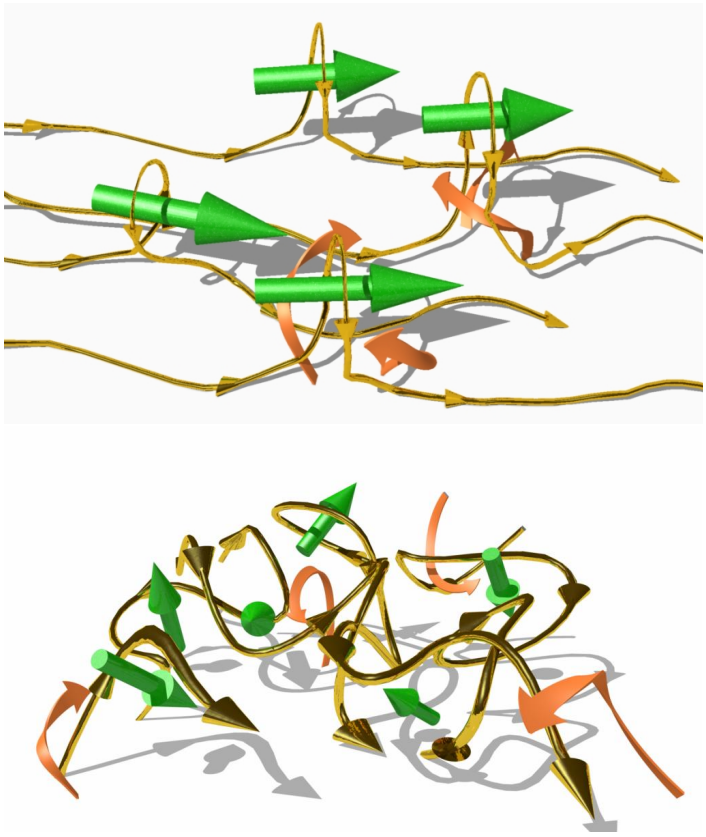

Figure 1.8 Illustration of constructive (top) and destructive (bottom) folding of a mean-magnetic field by a small-scale flow. In (A), radially-diverging cyclonic updrafts (orange flat arrows) create magnetic field loops with associated local electrical current density (green 3D arrows), as per Ampère's Law. If the field suffers relatively little deformation, then these local currents are oriented approximately parallel to the original mean magnetic field, and collectively add up to a mean current density parallel to the mean field. In (B), a "random" small-scale flow (orange flat arrows) acting on a mean magnetic field generate randomly-oriented magnetic field loops, with which are associated randomly-oriented local current densities; unlike in (A), these now vectorially add up to zero, but still contribute to enhanced Ohmic dissipation. Artwork kindly provided by D. Passos. {fig:folding}

From the dynamo point of view, the key addition made by the turbulent emf is the α-effect, because it allows to bypass Cowling's theorem. In the solar context, the break of reflection symmetry required to produce a non-

vanishing α-effect is imparted on the turbulent flow by the Coriolis force, with convective updrafts developing a systematic sense of twist, counter-clockwise (clockwise) in the Northern (Southern) solar hemisphere (Parker, 1955), much like cyclones in Earth's atmosphere, as illustrated schematically on Fig. 1.8A. Here a key dimensionless grouping is the *Rossby number*, measuring the influence of the Coriolis force on the small-scale flow:

Cyclonicity

Rossby number

$$\mathrm{Ro} = \frac{u}{2\Omega\, L} \ , \tag{1.47}$$

where u and L are typical velocity and length scales for the flow under consideration, and Ω is the solar angular velocity. Fluid motions acquire a cyclonic character in the $\mathrm{Ro} < 1$ regime, but not in the opposite situation where $\mathrm{Ro} > 1$. Deep convection, with $u \sim 10\,\mathrm{m\,s^{-1}}$ and $L \sim 10^7\,\mathrm{m}$, has $\mathrm{Ro} \sim 0.1$ and so is expected to acquire a cyclonic character, whereas surface convection is not ($u \sim 10^3\,\mathrm{m\,s^{-1}}$ and $L \sim 1000\,\mathrm{km}$ leading to $\mathrm{Ro} \sim 10^2$).

Imagine now the α-effect acting on a large-scale magnetic toroidal component. Geometrically, the zonally-directed magnetic fieldlines are lifted and twisted into meridional planes, as illustrated schematically on Fig. 1.8A. The combined effect of many such cyclonic events is to generate a magnetic component in meridional (r, θ) planes —or, equivalently, a zonally-oriented mean electrical current— where there was none originally (Parker, 1955); the net effect is thus to produce a large-scale poloidal magnetic component from a pre-existing large-scale toroidal component[5]. As explained earlier in §1.3.1, shearing of this poloidal magnetic component can in turn induce a toroidal component. Acting jointly, the α-effect and shearing by differential rotation can thus (in principle) produce a working dynamo loop, each mechanism providing the magnetic field component required by the other to operate. Of course, such a dynamo scenario is only viable provided turbulent induction wins over turbulent dissipation at large spatial scales.

1.3.5 The dynamo number

{ssec:dynnumber}

Consider a simple situation in which no large-scale flow is present and the large-scale magnetic component is force-free and given by Eq. (1.13); this is a reasonable approximation if no large-scale flow contributes to induction[6]. Assuming $\beta \gg \eta$ and with neither α nor β depending on position, the

[5] As with the STF dynamo encountered earlier (viz. Fig. 1.4), magnetic dissipation is again needed here, for the various loops to disconnect from the toroidal flux system and merge into a large-scale poloidal component.

[6] The small-scale magnetic component cannot be force-free, of course, otherwise no energy transfer from the flow to the magnetic field could take place, as per eq. (1.14).

substitution of eq. (1.13) into (1.43) immediately leads to:

$$\frac{\partial \langle \mathbf{B} \rangle}{\partial t} = k(\alpha - k\beta)\langle \mathbf{B} \rangle \ , \tag{1.48}$$ {eq:mfmhdff}

which accepts eigensolutions of the form:

$$\langle \mathbf{B} \rangle(\mathbf{x}, t) = \hat{\mathbf{b}}(\mathbf{x}) \exp(k(\alpha - k\beta)t) \ . \tag{1.49}$$ {eq:mfmhdff2}

Dynamo number

Growth of the magnetic field is only possible provided

$$D \equiv \frac{\alpha}{k\beta} > 1 \ . \tag{1.50}$$ {eq:mfmhdff3}

Critical dynamo number

The dimensionless combinaison of constant on the RHS of this expression defines the *dynamo number* (D) for this model; the *critical dynamo number* ($D_{\rm crit}$), here equal to unity, is the threshold value marking the onset of exponential growth. Remembering that k is an inverse length scale associated with $\langle \mathbf{B} \rangle$, this indicates that turbulent induction will tend to favor the growth of the eigenmode with the largest spatial scale than can be accomodated in the system, because the smaller magnetic scales are more strongly affected by dissipation[7]. Equation (1.49 also indicates that once D exceeds $D_{\rm crit}$, its value sets sets the growth rate of the magnetic field.

1.3.6 Dynamo waves

{ssec:dynwaves}

Now reintroduce a large-scale, uniformly sheared flow in the problem. To be specific, working in Cartesian geometry we write $\langle \mathbf{U} \rangle = \Omega z \hat{\mathbf{e}}_y$, and express the large-scale magnetic field as:

$$\langle \mathbf{B} \rangle(x, z, t) = \nabla \times (A(x, z, t)\hat{\mathbf{e}}_y) + B(x, z, t)\hat{\mathbf{e}}_z \ . \tag{1.51}$$ {eq:dynwav1}

Assuming again $\beta \gg \eta$, upon substituting this expression into the mean-field induction equation (1.43), the latter separates into:

$$\frac{\partial A}{\partial t} - \beta \left(\frac{\partial^2 A}{\partial x^2} + \frac{\partial^2 A}{\partial z^2} \right) = \alpha B \ , \tag{1.52}$$ {eq:dynwave2a}

$$\frac{\partial B}{\partial t} - \beta \left(\frac{\partial^2 B}{\partial x^2} + \frac{\partial^2 B}{\partial z^2} \right) = -\Omega \frac{\partial A}{\partial x} + \alpha \left(\frac{\partial^2 A}{\partial x^2} + \frac{\partial^2 A}{\partial z^2} \right) \ . \tag{1.53}$$ {eq:dynwave2b}

[7] These "smaller magnetic scales" characterizing $\langle \mathbf{B} \rangle$ are still much larger than those associated with the small-scale flow $\mathbf{u}'$ driving the α-effect and turbulent diffusivity, as per the assumption of scale separation.

With α, β and Ω independent of position and time, eigensolutions can be sought in the form of plane waves:

{eq:dynwave3}
$$\begin{bmatrix} A(x,z,t) \\ B(x,z,t) \end{bmatrix} = \begin{bmatrix} a \\ b \end{bmatrix} \exp[\lambda t + \mathrm{i}k(z\cos\vartheta + x\sin\vartheta)] \ . \tag{1.54}$$

where the wavenumber k sets the scale of the large-scale magnetic field, and ϑ the propagation direction in the $[x,z]$ plane. Substituting this expression into eqs. (1.52)–(1.53) leads to the dispersion relation

$$(\lambda + \beta k^2)^2 = \alpha k(\alpha k + \mathrm{i}\,\Omega\sin\vartheta) \ . \tag{1.55}$$ {eq:dynwave3}

This is a quadratic (complex) polynomial in λ, with the two solutions:

$$\lambda_\pm = -\beta k^2 \pm \sqrt{\frac{|\alpha|k}{2}}\Bigg\{\left(\sqrt{\Omega^2\sin^2\vartheta + \alpha^2k^2} + |\alpha|k\right)^{\frac{1}{2}} + \mathrm{i}\,\mathrm{sign}(\Omega\alpha\sin\vartheta)\,\left(\sqrt{\Omega^2\sin^2\vartheta + \alpha^2k^2} - |\alpha|k\right)^{\frac{1}{2}}\Bigg\} \ , \tag{1.56}$$ {eq:dynwave4}

The λ_- solution can only produce decaying disturbances ($\mathrm{Re}(\lambda_-) < 0$), whereas the λ_+ root can potentially leads to dynamo action, in the sense that $\mathrm{Re}(\lambda_+) > 0$. Examination of equation (1.56) indicates that an exponentially growing *dynamo wave* can materialize in a finite wavenumber "window" $k \in]0, k_*[$, where k_* is a root of: Dynamo wave

$$k_*^6 - \frac{\alpha^2}{\beta^2}k_*^4 - \frac{\alpha^2\Omega^2}{4\beta^4}\sin^2\vartheta = 0 \ . \tag{1.57}$$ {eq:dynwave5}

In the limit of strong shear ($|\alpha| \ll \sqrt{\beta|\Omega\sin\vartheta|}$, or, equivalently, if the second term on the RHS of eq. (1.53) is negligible with respect to the first, then we have

$$\mathrm{Re}(\lambda_+) \simeq -\beta k^2 + \sqrt{\frac{|\alpha\Omega\sin^2\vartheta|k}{2}} \ , \tag{1.58}$$ {eq:dynwave6}

and exponential growth of the magnetic field will thus take place provided

$$\frac{|\alpha\Omega\sin\vartheta|}{2\beta^2k^3} > 1 \ . \tag{1.59}$$ {eq:dynwave7}

with the root of eq. (1.57) then given by

$$k_* \simeq \left(\frac{|\alpha\Omega\sin\vartheta|}{2\beta^2}\right)^{1/3} \ . \tag{1.60}$$ {eq:dynwave8}

The LHS of eq. (1.59) thus acts as the dynamo number for this dynamo wave solution, with a critical value of unity. Once again we find that the

larger scales (small k) are favored by the dynamo process. Equation (1.57) indicates that the window of dynamo action is widest, and eq. (1.58) that the growth rates largest, for $\vartheta = \pi/2$; i.e., for a wavevector oriented in x, along isolines of $\langle \mathbf{U} \rangle$.

The eigenvalues associated with these growing solutions have nonzero imaginary parts, so that the combined action of large-scale shear (Ω), turbulent induction (α) and turbulent dissipation (β) can generate propagating magnetic "waves", leading to local reversals of magnetic polarity every half-wave period (Parker, 1955). In this shear-dominated regime the frequency of these so-called dynamo waves is given by

{eq:dynwave9}

$$\mathrm{Im}(\lambda_+) \simeq \mathrm{sign}(\Omega\alpha \sin\vartheta) \sqrt{\frac{|\alpha\Omega \sin\vartheta| k}{2}} \ . \tag{1.61}$$

Sign rule

The sign of the product $\alpha\Omega$ thus sets the propagation direction along the $\langle \mathbf{U} \rangle$ isolines. This is known as the *Parker-Stix-Yoshimura* sign rule, and carries over to models in non-cartesian geometries with dynamo coefficients varying with position (see Stix, 1976; Yoshimura, 1975). Here if we associate z with the radial direction and $\langle \mathbf{U} \rangle$ with differential rotation ($y \equiv$longitude), this implies dynamo waves propagating in the latitudinal direction, in qualitative agreement with the sunspot butterfly diagram (REF to later section).

REF to Fig in other chapter

Such dynamo waves will indeed materialize in mean-field dynamo models investigated in chapter 2.

In the opposite limit $\Omega \to 0$, the imaginary part of the eigenvalue vanishes (viz. eq. (1.56)), eq. (1.55) leads to a condition for exponential growth ($\lambda > 0$) identical to eq. (1.49), as expected.

{ssec:BL}

1.3.7 Active region decay and the Babcock-Leighton mechanism

Large bipolar magnetic regions (herefater BMR) are believed to result from the buoyant destabilisation and rise to the photosphere of toroidal magnetic flux ropes having formed from the diffuse magnetic field in the deep solar interior, at or immediately beneath the interface between the convection zone and underlying stably stratified radiative core (Parker, 1975; Moreno-Insertis, 1986; Choudhuri and Gilman, 1987; Fan, 2009). BMRs are observed to emerge with their magnetic axis approximately aligned with the solar E-W direction of rotation and show an ordering of magnetic positive/negative polarities that is the same within an hemisphere, opposite across hemisphere, and that switches from one activity cycle to the next. These are known as Hale's polarity Laws, and indicate that the deep-seated solar magnetic field is antisymmetric about the equatorial plane.

Magnetic flux rope

REF to appropriate obs Fig

The magnetic axes of BMRs are not exactly aligned with the E-W direction. Despite a large scatter in observed tilt angles, on average BMRs exhibit a systematic tilt with respect to the E-W direction, the leading member of the pair (with respect to the direction of rotation) being closer to the equator than the trailing member. This tilt angle increases with heliospheric latitude, a pattern known as Joy's Law (Hale et al., 1919; Dasi-Espuig et al., 2010; Stenflo and Kosovichev, 2012; McClintock and Norton, 2013; **?**). The tilt is believed to arise from the action of the Coriolis force on the secondary flow developing along the rising flux tube as a consequence of angular momentum conservation (Fan et al., 1993). Models using the thin flux tube approximation succeed in reproducing this tilt pattern (Fan et al., 1993; D'Silva and Choudhuri, 1993; Caligari et al., 1995).

Joy's Law

The tilt of the magnetic axis of a BMR implies a non-zero projection along the N-S direction, which amounts to a dipole moment. For a BMR of unsigned magnetic flux Φ emering at latitude λ, with the two poles separated by an angular distance d and with a tilt angle α with respect to the E-W direction, the dipole contribution δD is given by:

$$\delta D = \frac{3d\cos\lambda}{4\pi R^2}\Phi\sin\alpha\ . \tag{1.62}$$ {eq:thenumber}

The decay of this BMR and subsequent dispersal of its magnetic flux by surface flows can release a fraction of this dipole moment and contribute to the global solar dipole. This occurs because the leading members of each pair is subjected to greater cross-equatorial diffusive cancellation than the trailing member, leading to an excess of trailing polarity accumulating at high latitudes (DeVore et al., 1984; Cameron et al., 2013; Jiang et al., 2014). This process is clearly observed in synoptic magnetograms (Ref to Hathaway Fig). The net effect of the emergence and decay of many such BMRs is thus the production of a dipole moment (poloidal field) from decaying active regions (emerging toroidal field). This toroidal-to-poloidal magnetic regeneration process is known as the Babcock-Leighton mechanism, after Babcock (1961) and Leighton (1964). Together with shearing by differential rotation, it can yield a working dynamo loop.

REF to a synoptic magnetogram

Figure 1.9 shows results of a simulation (Lemerle et al., 2015) of surface magnetic flux evolution throughout activity cycle 21 (1976–1986), using observed active region emergences as input. The bottom panel is grayscale rendering of the synoptic (zonally-averaged) magnetogram for the radial magnetic component. The salt-and-pepper pattern at low latitudes reflects the emergence of bipolar magnetic regions, which do not zonally average out to zero on this synoptic magnetogram because of their tilt with respect

Surface flux transport

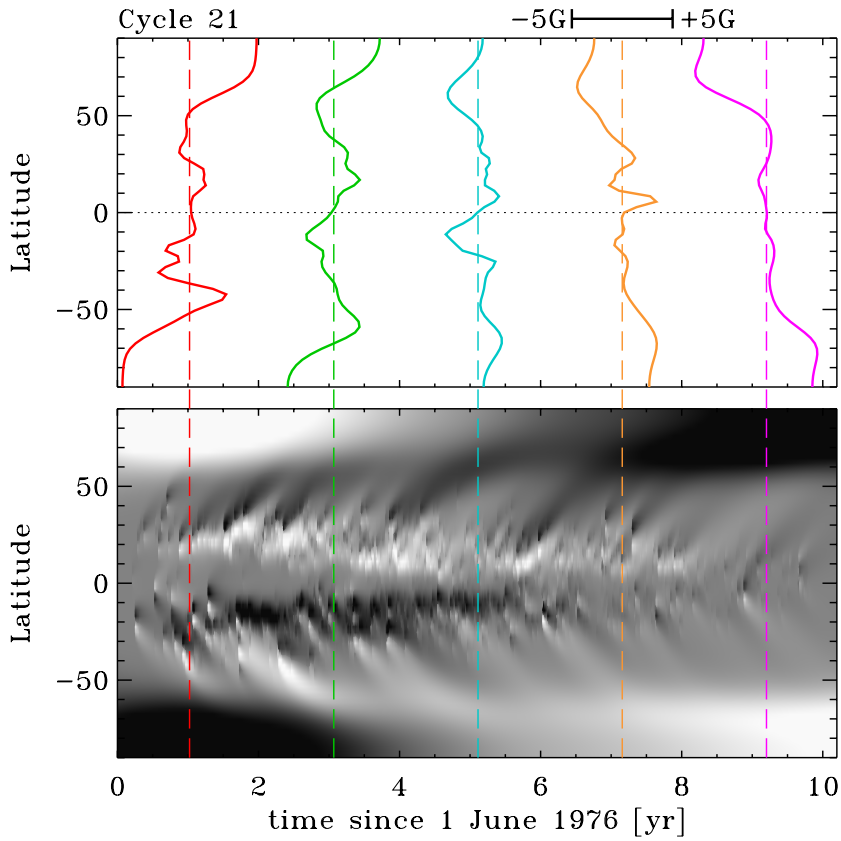

Figure 1.9 A simulation of solar surface magnetic flux evolution showing the Babcock-Leighton mechanism in action, in response to emergence of bipolar magnetic regions in the course of activity cycle 21 (1976–1986). The bottom panel shows the corresponding synthetic synoptic (zonally-averaged) magnetogram, with the vertical lines flagging the five times at which the temporal cuts are plotted on the top panel. The grayscale is saturated at ±5 G to better emphasize the poleward transport at mid-latitudes. Surface flux evolution simulation taken from Lemerle et al. (2015), using as input the cycle 21 active region emergence database of Wang and Sheeley (1989).

{fig:BLmech}

to the East-West direction. The poleward transport of the trailing polarity shows up as slanded streaks, black (negative B_r) in the Northern hemisphere and white (positive B_r) in the South. This eventually leads to the reversal of the positive dipole of the initial condition, occuring here about 5 years

after the beginning of the simulation. This is followed by the buildup of the negative dipole, peaking close near the end of the simulation at polar field strength approaching 10^{-3} T. A different view of the dipole is presented on the top panel, showing latitudinal cuts of the zonally-averaged surface radial magnetic field spaced 25 months apart, as color-coded. Note the steep cross-equatorial gradient in B_r building up and sustained throughout the rising and maximum phases of the sunspot cycle, leading to diffusive cancellation of the leading polarity flux (DeVore et al., 1984).

The Babcock-Leighton mechanism is definitely observed operating at the solar surface, and models of surface magnetic flux evolution can reproduce quite well observed synoptic magnetograms; see, e.g., (see, e.g., Wang et al., 1989; Wang and Sheeley Jr, 1991; Schrijver et al., 2002; Baumann et al., 2004; Jiang et al., 2014; Upton and Hathaway, 2014; Lemerle et al., 2015); consequently the Babcock-Leighton mechanism is very well-constrained observationally. The key remaining question is whether it is a crucial component of the dynamo loop, or represents a mere side-effect of a dynamo operating independently in the solar interior.

The solar polar cap magnetic flux adds up to $\sim 10^{14}$ Wb, which is equivalent to the unsigned flux contained in one large bipolar magnetic regions. Now, about 10^{17} Wb of magnetic flux emerges in such active regions in the course of a typical activity cycle, so the toroidal-to-poloidal flux conversion efficiency required of the Babcock-Leighton mechanim is quite low. The poloidal flux so produced would in itself be sufficient to account for the magnetic flux emerging in all active regions in a cycle, considering the amplitude of the observed differential rotation (on this point see also Cameron and Schüssler, 2015).

1.3.8 HD/MHD instabilities {ssec:instabil}

In the mildly stably stratified upper tachocline, immediately beneath the base of the solar convection zone, the presence of differential rotation and strong magnetic fields is conducive to the growth of a number of hydrodynamical and magnetohydrodynamical instabilities. Under the action of the Coriolis force, the growth of these instabilities can generate flows with a net helicity which, upon acting on a pre-existing large-scale magnetic field, can produce a field-aligned electromotive force reminiscent of the α-effect (see, e.g., Ferriz-Mas et al., 1994; Ossendrijver, 2000a; Thelen, 2000; Dikpati and Gilman, 2001; Chatterjee et al., 2011). The effect of these various instabilities is usually invoked to provide the zonal electromotive force required to regenerate the poloidal large-scale component, with shearing of

this poloidal component by the tachocline differential rotation (viz. §1.3.1) invoked to close the dynamo loop.

{sec:fluxt}

1.4 Magnetic flux transport

The advection term on the RHS of eq. (1.29) cannot, in itself, act as a dynamo, but the associated transport of the magnetic field can be an essential component in any dynamo models where the two source regions for the $T \to P$ and $P \to T$ mechanisms are spatially segregated; coupling is required for a working dynamo loop to ensue.

On large scales, the meridional flow pervading the solar convection zone is a potentially important contribution to magnetic flux transport, acting as a "conveyor belt" linking the surface layers to the tachocline. As with differential rotation, this flow is ultimately driven by convective turbulence, and is intimately coupled to the internal rotation profile via the mechanism known as gyroscopic pumping (see Featherstone & Miesch 2015). This axisymmetric ($\partial/\partial\phi \equiv 0$) flow is oriented within meridional planes $[r, \theta]$, and is directly observed at the solar surface, poleward at speeds reaching at $\sim$ 10–20 m s^{-1} at mid-latitudes (Komm et al 1993; Ulrich 2010, Hathaway & Rightmire 2010). This poleward transport is clearly visible on the surface flux transport simulation of Fig. 1.9, as it leads to the slanting structures extending from active regions latitudes to the polar caps. Mass conservation requires an equatorward return flow somewhere in the solar interior, but the exact shape of this return flow remain unknown. The minimal assumption is of a single cell per meridional quadrant, with the equatorward return flow peaking near the base of the convective envelope. This is the profile most often used in extant flux transport dynamo models, and has received support from some helioseismic inversions of large-scale solar internal meridional flows (Rajaguru and Antia, 2015; **?**; Mandal et al., 2018). Other such inversions suggest a more complex picture, with multiple flow cells stacked in radius and perhaps latitude (Schad et al., 2013; Zhao et al., 2013; Jackiewicz et al., 2015; **?**). Correlation tracking of magnetic features at supergranular scales also suggest a shallow equatorward return flow (Hathaway, 2012), which of course does not rule out deeper flow cells.

Within the framework of mean-field magnetohydrodynamics (§1.3.4), and from the viewpoint of the large-scale magnetic field, the advective contribution of the small-scale convective turbulence becomes subsumed in two distinct effects, embodied in the $\boldsymbol{\gamma}$ and $\boldsymbol{\beta}$ terms in the expansion (1.36). The first, turbulent pumping, acts as an additional contribution to the large-scale flow $\langle \mathbf{U} \rangle$ on the RHS of the mean-field induction equation (1.32). This is

a non-solenoidal ($\nabla \cdot \boldsymbol{\gamma} \neq 0$) pseudo-flow, in the sense that it acts as such only on the large-scale magnetic field $\langle \mathbf{B} \rangle$. The second advective contribution of the small-scale flow becomes turbulent diffusion of $\langle \mathbf{B} \rangle$. As discussed in §1.3.4, turbulent diffusion globally destroys the large-scale magnetic field $\langle \mathbf{B} \rangle$ through the enhanced dissipation of the current density supporting it; but it can also lead to the diffusive transport of magnetic flux from regions of strong magnetic fields to regions devoid of magnetism. Indeed, turbulent diffusion also contributes significantly to the poleward transport of surface magnetic fields on Figure 1.9.

Numerical simulations of MHD convection and dynamo action, to be reviewed in §2.1, indicate that meridional flow and turbulent pumping speeds can reach meter-per-second values in the bottom half of the solar convection zone, of the same order of magnitude as the phase speed of dynamo waves (§1.3.6). These transport mechanisms can thus contribute, and perhaps even dominate, the equatorward progression of activity belts as the activity cycle unfolds, and under some circumstances even set the magnetic cycle period. Dynamo models achieving equatorward propagation based on these flux transport mechanisms are discussed in chapter 2.

1.5 More on timescales {sec:moretimescl

Through the survey of MHD inductive and advective mechanisms just completed, various timescales for magnetic field evolution have been encountered. Diffusive timescales for the large-scale magnetic field can vary from at least 10^6 yr in turbulence-free regions such as the lower tachocline, down to tens of years in the upper convection zone due to strongly enhanced dissipation mediated by convective turbulence. Advective timescales associated with thermally-driven convection range from 10 minutes for surface convection, up to around a month near the bottom of the solar convection zone. Differential rotation is characterized by advective timescales of order one year, while the advective timescale of the meridional flow ranges from a few years at the surface, up to a few tens of year for the turnover time of a single cell flow reaching all the way to the base of the convective envelope. Dynamical timescales associated with the action of the Lorentz force on inductive flow can also vary over many orders of magnitude, according to magnetic field strengths and physical conditions in the region(s) of the solar interior over which the backreaction is taking place.

This wide range of timescales available to the flow-field dynamo system implies that modulation of the magnetic cycle can take place over an equivalently wide range of timescales, according to the nature of the physical

mechanism(s) dominating the amplification, transport and dissipation of magnetic fields, and of the nonlinear backreaction mechanisms responsible for regulating the amplitude of the cycle.

1.6 Summary

1. The spatiotemporal evolution of magnetic fields in solar/stellar interiors is well-described by magnetohydrodynamics;
2. A flow is deemed a dynamo if its inductive action can amplify and sustain the magnetic field against Ohmic dissipation;
3. Thermally-driven fluid flows are the ultimate energy source powering solar and stellar dynamos and driving the solar magnetic cycle;
4. A number magnetohydrodynamical inductive mechanisms can achieve magnetic field amplification and regeneration in the sun: shearing by differential rotation, cyclonic turbulence in the convection zone, surface decay of active regions, fluid and/or MHD instabilities in the outer reaches of the radiative core;
5. Small-scale dynamos generate magnetic fields on scales comparable or smaller than those of the inductive flow, but no magnetic flux on larger scales;
6. Large-scale dynamos generate net magnetic flux on spatial and temporal scales larger than those of the inductive flows.

Magnetic field induction, transport, dissipation, and dynamical backreaction on the inductive flows jointly operate over a very wide range of characteristic timescales, implying system response over a similarly wide range of timescales.